Check for updates

Colloidal transport in bacteria suspensions: from bacteria collision to anomalous and enhanced diffusion

Antoine Lagarde,†[a] Noémie Dagès,†[a] Takahiro Nemoto,‡[b] Vincent Démery, [ID][ac] Denis Bartolo[a] and Thomas Gibaud [ID] *[a]

Swimming microorganisms interact and alter the dynamics of Brownian particles and tend to modify their transport properties. In particular, dilute colloids coupled to a bath of swimming cells generically display enhanced diffusion on long time scales. This transport dynamics stems from a subtle interplay between the active and passive particles that still resists our understanding despite decades of intense research. Here, we tackle the root of the problem by providing a quantitative characterisation of the single scattering events between a colloid and a bacterium, a smooth running *E. coli*. Based on our experiments, we build a minimal model that quantitatively predicts the geometry of the scattering trajectories, and enhanced colloidal diffusion at long times. This quantitative confrontation between theory and experiments elucidates the microscopic origin of enhanced transport. Collisions are solely ruled by stochastic contact interactions and the ratio of the drag coefficients of the colloid and the bacteria. Such description accounts both for genuine anomalous diffusion at short times and enhanced diffusion at long times with no ballistic regime at any scale.

1 Introduction

In nature, virtually all swimming microorganisms rely on interactions with particles dispersed in their natural environments. Prominent examples include protists grazing on microscopic preys, and sperm cells fertilizing ovocites. In the labs, researchers have successfully put synthetic and living microswimmers to work to achieve a dynamics out of reach of equilibrium systems, including the assembly and actuation of micromachines,[1–4] topological-defect healing in colloidal crystals,[5] and enhanced transport in non-Brownian suspensions. This latter line of research goes back to one of the earliest active-matter experiments.[6] Investigating the diffusion of colloidal particles dispersed in a liquid film hosting swimming bacteria, Wu and Libchaber laid out the foundation of active transport, and made seemingly simple observations that remain controversial despite twenty years of intense research.[7]

When passive colloidal particles are dispersed in a dilute solution of motile organisms, they display a generic two-time dynamics. At long times, regardless of the nature of the swimming particles, the multiple uncorrelated interactions between the active and passive units result in an enhanced diffusive dynamics characterized by a Gaussian displacement statistics.[6–10] Micron-size colloids dispersed in a suspension of *E. coli* can diffuse as fast as nanoparticles in water. By contrast, at short times, the transport dynamics does not map to equilibrium and is generically non-Gaussian and superdiffusive. This anomalous dynamics is however non-universal and was the subject of contradictory reports. One situation was thoroughly investigated by the group of Polin, who established the ballistic nature of colloid transport in situations where the passive particles are much smaller than the active units.[9,11] In this particular case, the swimmers Chlamydomonas reinhardtii entrain the colloid, which leads to a ballistic motion of the colloid.

Conversely, when the size of the passive objects compares or exceeds that of the swimming particles, the situation remains elusive and controversial. Both the early experiments by Wu and Libchaber (*E. coli*), and the more recent results by Valeriani *et al.*[12] (*B. subtilis*) clearly demonstrated a non-ballistic regime at short time scales. However a plethora of theories and numerical simulations predict short-time ballistic transport with no consensus on the relative contribution of the swimmer hydrodynamic and contact interactions, see *e.g.*[13–18] and references therein.

[a] *Univ Lyon, Ens de Lyon, Univ Claude Bernard, CNRS, Laboratoire de Physique, F-69342 Lyon, France. E-mail: thomas.gibaud@ens-lyon.fr*

[b] *Philippe Meyer Institute for Theoretical Physics, Physics Department, École Normale Supérieure & PSL Research University, 24 rue Lhomond, F-75231 Paris Cedex 05, France*

[c] *Gulliver, UMR CNRS 7083, ESPCI Paris, PSL Research University, 10 rue Vauquelin, 75005 Paris, France*

† These authors contributed equally to this work.

‡ Current affiliation: Mathematical Modelling of Infectious Diseases Unit, Institut Pasteur, 25-28 Rue du Docteur Roux, 75015 Paris, France.

To date, the only available explanation for the anomalous diffusion of passive particles coupled to active baths relies on the emergence of collective motion and therefore does not apply to the vast majority of experiments performed in dilute suspensions.[6,19] The current status is that most experiments on active transport are now analysed implicitly assuming a crossover between a ballistic and a diffusive regime.[12,20,21] The primary reason for this rather confusing situation is twofold. Firstly, we lack a clear characterization and understanding of the microscopic scattering dynamics ruling the couplings between active-swimmer baths and passive particles. Secondly, the low temporal resolution and small dynamical range of the control parameters hinder the quantitative characterization of the asymptotic statistics in the current state-of-the-art experiments.

In this article, we rectify this situation investigating the enhanced transport of colloids in *E. coli* suspensions. We first provide a comprehensive characterization of the collisions between a swimming bacteria and passive colloidal beads, and introduce a minimal theoretical model that faithfully account for their full scattering dynamics. Our model rules out the impact of the swimmer far-field hydrodynamic interactions in favour of close contact interactions and the ratio of the drag coefficient of the colloid over the drag coefficient of the bacteria. Investigating the consequences of this scattering process on active transport, we firmly establish the existence of genuine superdiffusion and non Gaussian transport at short time, revealing a complex interplay between the propulsion of the active units and the displacements of the passive colloids upon physical collisions.

2 Experimental setup

We provide a thorough description of our experiments in the Methods section 6. In brief, our experimental system is composed of an aqueous dispersion of bacteria seeded with polystyrene colloids of radius $\ell_c = 2.5$ μm or $\ell_c = 5$ μm. Due to density mismatch with the background fluid, the colloids sediment on the bottom plate of the observation cell leading to a quasi two-dimensional system where their dynamics is observed using video-microscopy. The colloids diffuse in the (xy) plane. Using a particle tracking algorithm we measure a free diffusion coefficient $D_0(\ell_c = 2.5$ μm$) = 0.015$ μm^2 s^{-1} and $D_0(\ell_c = 5$ μm$) = 0.0075$ μm^2 s^{-1}.

The bacteria are fluorescent smooth-runner mutants RP437 of *E. coli*. They are smaller than the passive colloids, measurements of their average diameter is 0.5 μm and their average length is $L_b = 4.3 \pm 2$ μm, values comparable to the literature.[22] Bacteria suspensions are prepared according to the protocols reviewed in ref. 22. Using standard single particle tracking,[23] we find that the bacteria swim at an average speed $v_b = 15 \pm 4$ μm s^{-1}. In order to run experiments long enough to achieve large-enough statistics, the bacteria solutions are placed in agar observation cells as sketched in Fig. 1(a). Using differential dynamic microscopy (DDM),[24–26] we measured the average bacteria velocity of concentrated bacteria dispersion to test the life expectancy of the bacteria in different observation cells. The primary advantage of agar-based devices is that the bacteria remain alive and active with stationary
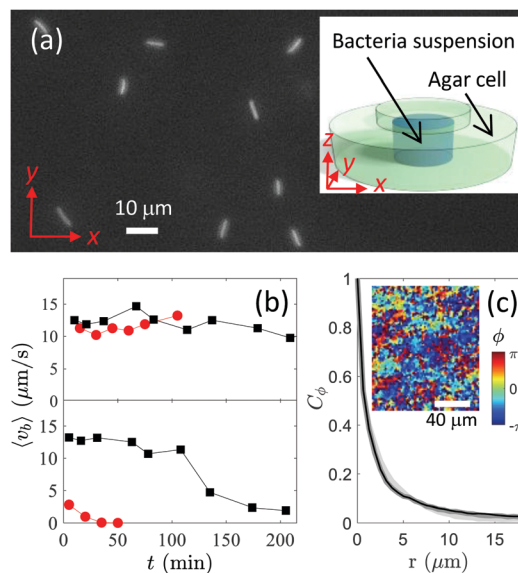

Fig. 1 Bacteria suspension. (a) Fluorescence microscopy image of a dilute bacteria suspension. Inset: Sketch of the agar observation cell. (b) Average bacteria velocity v_b measured using DDM (Fig. 7) as a function of the age of the solution in the agar cell (square) and in a standard cover-slip observation cell (circle) for two bacteria concentrations $c = 1.8 \times 10^{10}$ mL^{-1} (top) and $c = 18 \times 10^{10}$ mL^{-1} (bottom). (c) Correlation function of the velocity-field orientation ϕ plotted as a function of the distance r for concentrations $c = 2$ (light grey), 10 (dark grey) and 20×10^{10} mL^{-1} (black). Inset: The instantaneous orientation shows very little spatial correlation ($c = 18 \ 10^{10}$ mL^{-1}).

dynamics over more than 100 min, in contrast to standard glass or PDMS cells where the bacteria average velocity decays monotonically and can vanish in ∼10 min, see Fig. 1(b). Using particle image velocimetry (PIV) on bright field images, we measure the velocity field in pure bacteria suspensions. Varying the bacteria concentrations c from 10^7 to 3×10^{11} mL^{-1}, we never observe spatial correlations in the active flows, Fig. 1(c): the bacteria dispersion is an isotropic active fluid at all concentrations considered in this work. The bacteria concentration is however not homogeneous. It displays a concentration gradient along the vertical direction: due to interactions with the observation cell's wall, bacteria are more numerous at the bottom and the top of the observation cell.[27] The bacteria concentration c used in the following corresponds to the one measured at the bottom of the observation cell. Using simultaneously a bright field microscopy for the colloids and fluorescence microscopy for the bacteria, we record videos of dilute colloidal dispersions in presence of bacteria ∼2 μm above the bottom of the observation cell.

3 Bacteria-colloid collisions

3.1 Experimental results

We start by analysing the collisions between a single colloid of radius $\ell_c = 5$ μm and a single bacterium, see Fig. 2(a). Combining bright field and fluorescence microscopy makes it possible to simultaneously track instantaneous positions of the colloid, $\mathbf{r}_c(t) = (x_c(t), y_c(t))$, and of the colliding bacterium, $\mathbf{r}_b(t) = (x_b(t), y_b(t))$.
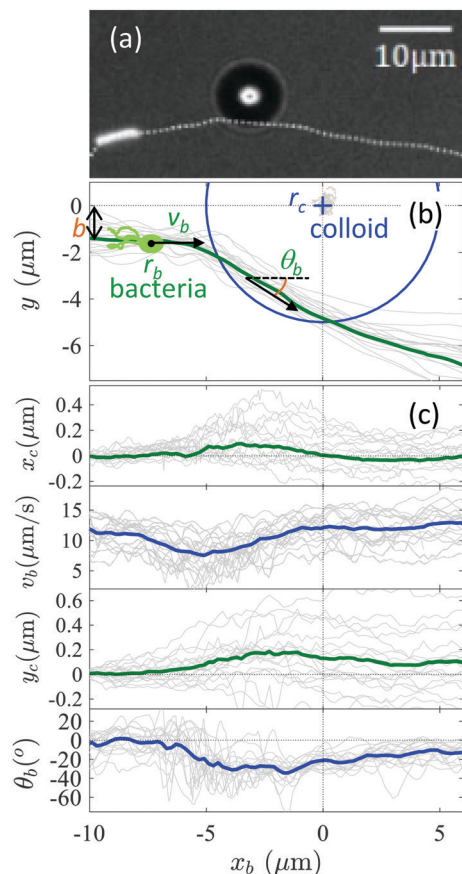
Fig. 2 Collision between a bacterium and a colloid. (a) Typical microscopy image of a collision. (b) The bacteria at position $\mathbf{r}_b(x_b,y_b)$ has a velocity v_b. b is the $y-$ distance to the center of the bacteria taken at $x_b = -10$ μm. At $x_b = -10$ μm the velocity v_b is oriented along the $x-$ axis. The colloid of radius $\ell_c = 5$ μm is characterized by the position of its center of mass $\mathbf{r}_c(x_c, y_c)$. The bacteria trajectory is deviated by the colloid by an angle θ_b. Grey lines indicate individual quantities and the green or blue lines are the average quantities. (c) Collision parameters x_c, y_c, v_b and θ_b as a function of x_b.

Fig. 3 Averaged collisions as a function of the impact parameter b. The average is performed on 10 to 100 collision events. (a) Averaged trajectories of the bacteria during a collision. The color codes for different b values. (b) Maximum deviation of the center of the colloid (x_c^M (triangle), y_c^M (square)), maximum relative velocity drop, $\Delta v_b/\langle v_b \rangle$ (diamond) and maximum deviation angle θ_b^M (circle) as a function of b; the maxima are computed on the averaged trajectories. Red lines are model predictions.

To characterize the collision process, we choose the time origin when the bacterium and the colloid are separated by a distance of 10 μm. The spatial origin and orientation of the frame are then set so that $\mathbf{r}_c(t = 0) = 0$, and $\hat{\mathbf{y}} \cdot \mathbf{v}_b(t = 0) = 0$, where $\mathbf{v}_b(t)$ is the instantaneous bacterium velocity, see Fig. 2(b). The impact parameter of the collision is then defined as $b = y_b(t = 0)$, Fig. 2(b).

Taking the bacterium position along the x-axis, x_b, as the parameter for both the bacterium and colloid trajectories, we monitor the displacement of the colloid (x_c, y_c) as well as the speed v_b and deviation angle θ_b of the bacterium, Fig. 2(b) and (c). Comparing the scattering trajectories of hundreds of bacteria, and grouping those corresponding to the same impact parameter b, we identify a set of robust features. Both the colloids and the bacteria trajectories fluctuate around well-defined average paths. For a parameter $b = -1.5$ μm, the average path of both the bacterium and the colloid is clearly affected by the collision. The bacterium tends to push the colloid: $x_c > 0$ and $y_c > 0$ and the colloid slows down the bacterium and deviate its trajectory by an angle $\theta_b < 0$ (when $b < 0$).
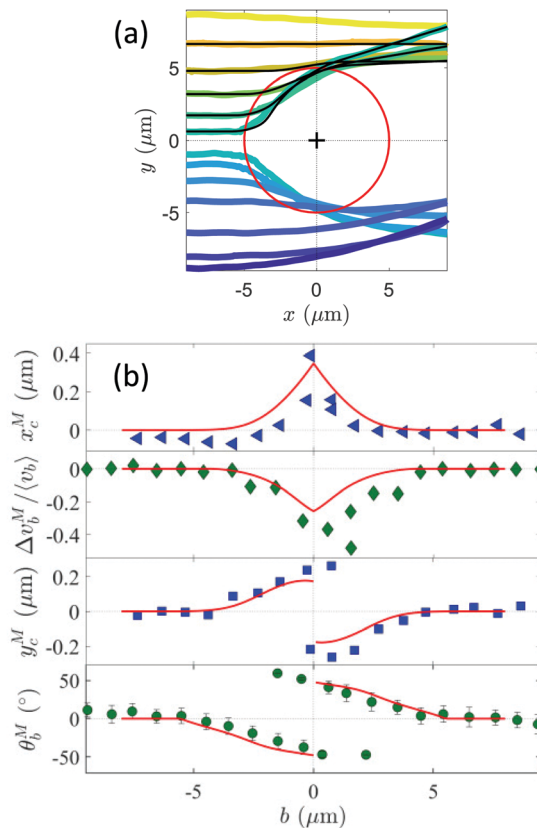
Given the radial symmetry of the colloidal particles, the average dynamics is accurately determined by the sole impact parameter b, Fig. 3(a). In order to quantify this scattering, we plot, as a function of b, in Fig. 3(b), the maximum displacements of the colloid along the x and y directions (x_c^M, and x_c^M) as well as the maximum velocity drop $\Delta v_b^M = v_b^M - \langle v_b \rangle$ and deviation angle θ_b^M of the bacterium trajectories. Those maxima are reached around $x_b \sim -2$ μm, except for the velocity drop which takes place around $x_b \sim -5$ μm, Fig. 2(c).

From Fig. 3(b), we readily infer four essential results. (i) We find no average displacement of the colloidal particle when the impact parameter exceeds one colloid radius: the interactions between the colloids and the bacteria are short ranged. We can therefore discard the role of far-field hydrodynamic interactions in the collision process. (ii) On the contrary, for $|b| < 5$ μm, the bacterium and colloid trajectories are affected. The scattering of each bacterium is systematically associated to a net displacement of the colloid over distances significantly larger than its typical diffusion length over the collision time. The colliding bacterium pushes the colloid away from its initial position. We indeed find that x_c^M is positive and that y_c^M and b have opposite signs for all impact conditions. The effect is maximal for a frontal

collision, $b \sim 0$. (iii) The bacterium slows down upon contact and the reduction of its swimming speed Δv_b^M mirrors the magnitude of the colloid displacements. This effect is also maximal for $b \sim 0$, where the relative velocity drop is around 40%. (iv) The bacterium is mostly scattered upward if $b > 0$ and downward if $b < 0$. The scattering angle of the bacterium trajectories θ_b^M is maximal upon head-on collisions ($b \sim 0$) and reaches a value of $50°$. We never observe any orbital trajectory akin to that observed using synthetic active colloids or when *E. coli* collides cylindrical posts.[28–30] These last two observations further confirm the prominence of contact or lubrication interactions in the collision dynamics. This vouch for steric repulsion between the colloid and the bacterium and exclude hydrodynamic interactions, which would lead to an effective attraction along the y-direction due to the pusher nature of the swimmer.[31]

3.2 Theoretical description of bacteria-colloid scattering

In order to account for our planar optical measurements, we describe the 3D collision between a bacterium and a colloid by an effective two-dimensional model using the collision dynamics of two disks with different radii, $\ell_b = 0.25$ μm (for the bacterium) and $\ell_c = 5$ μm (for the colloid), positioned at r_b, r_c. This model therefore neglects that bacteria may collide with the colloid at different altitude z and that the trajectory can be tilted with respect to the xy-plane. Given the vertical gradient in bacteria concentration, it also neglects the fact that collisions are less likely as z increases. Their dynamics are described by the two over-damped equations:

$$\frac{dr_b}{dt} = v_b \hat{e} + \frac{1}{\gamma_b} F_{int}^b, \quad \frac{dr_c}{dt} = \frac{1}{\gamma_c} F_{int}^c. \quad (1)$$

where γ_b and γ_c are the drag coefficients of the bacterium and the colloid, respectively. We assume an isotropic drag coefficient for the bacterium to keep the model as simple as possible. The drag coefficient of the colloid can be deduced from its diffusion coefficient using Einstein relation: $D_0 = 0.0075$ μm^2 s^{-1}, leading to $\gamma_c = k_B T/D_0 = 5.5 \times 10^{-7}$ Ns m^{-1}.

In eqn (1), $v_b = 15$ μm s^{-1} is the typical velocity of the bacteria far from the colloid and $\hat{e} = (\cos\theta, \sin\theta)$ is a unit vector that defines its orientation. We model the bacterium-colloid repulsive interaction by the forces F_{int}^b, F_{int}^c both deriving from the same contact potential

$$F_{int}^{c,b} = -\frac{\partial}{\partial r_{c,b}} U(|r_c - r_b|), \quad (2)$$

where $U(r)$ is the Weeks–Chandler–Andersen potential of range $r_0 = 2^{1/6}(\ell_b + \ell_c)$ and magnitude ε:

$$U(r) = \varepsilon \left[\left(\frac{r_0}{r}\right)^{12} - 2\left(\frac{r_0}{r}\right)^6 + 1 \right] \Theta(r_0 - r), \quad (3)$$

Since we aim at understanding the average properties of the collision, we do not introduce noise in our model, while noise is obviously present in the experiments as can be seen from the dispersion of the (grey) trajectories in Fig. 2. Guided by our experimental observations, we also introduce a torque that aligns the orientation of the bacterium $\hat{e}$ with the surface of the colloid during a collision, Fig. 2(b) and 3(b). Denoting by θ_{tan} the angle between $\hat{e}$ and the vector tangent to the colloid surface, the overdamped orientational dynamics of the bacterium reads

$$\frac{d\theta}{dt} = \Gamma \sin(\theta_{tan}) \Theta(r_0 - |r_c - r_b|), \quad (4)$$

where Γ is the reorientation rate that sets the amplitude of the torque, and r_0 is the effective range of the aligning torque, taken identical to that of $U(r)$ for the sake of simplicity. We note that eqn (4) differs from the models introduced in ref. 29 and 30 where the angular dynamics selects a preferred finite angle with the solid surface, thereby promoting circular orbits. As we observe no orbiting trajectory we neglect this contribution.

We determine the parameters $\varepsilon = 0.41 k_B T$, $\Gamma = 3.35$ s^{-1} and $\gamma_b = 1.7 \times 10^{-7}$ Ns m^{-1} by fitting the model to the experimental data of single collision trajectories as a function of the impact parameter b, Fig. 3(a). Since ε enters in the model only in the combinations ε/γ_b and ε/γ_c, its value is unimportant and what matters for the trajectories is the ratio of the drag coefficients, γ_b/γ_c. The value of the drag coefficient obtained for the bacterium is higher than previously reported values: 0.31×10^{-7} Ns m^{-1}.[32] The differences may be attributed to the difference of bacteria type, a more viscous environment and proximity to the cell floor.

Using these fitting parameters, we calculate the collision parameters x_c, y_c, $\Delta v_b/v_b$, θ_b for all values of b. Note that the small repulsion parameter allows for the bacterium to "penetrate" into the colloid (Fig. 3(a)); this comes from the projection of three dimensional trajectories onto the observation plane, whereby bacteria passing above or below the colloid are pictured "inside" the colloid. As shown in Fig. 3(b), the trajectories predicted from this minimal model quantitatively capture the average properties of the collision for all impact parameter values. We note that the model remains robust upon small variations of the bacteria radii ℓ_b.

4 Colloids dynamics as a function of the bacteria concentration

4.1 Mean square displacement

We now turn our attention to the enhanced transport dynamics of the passive colloids animated by thermal fluctuations and collisions with the swimming cells. We use colloids of radius $\ell_c = 2.5$ μm. The colloid concentration is kept very low to avoid colloid–colloid interactions: 3.6×10^{-4} colloids μm^{-2} corresponding to an area fraction of 0.007. To characterise the colloids motion, we record movies of colloids dispersed in bath of bacteria at a concentration c and we track their trajectory r_c as a function of time. At $c = 0$, the colloids are weakly Brownian: the mean square displacement (MSD) of the colloids evolves linearly with the lag time Δt as shown in Fig. 4(a), and we measure a free diffusion coefficient of $D_0 = 0.015$ μm^2 s^{-1}.

As shown in Fig. 4(a), upon increasing the bacteria concentration, the MSD becomes larger as c increases. In order to pinpoint
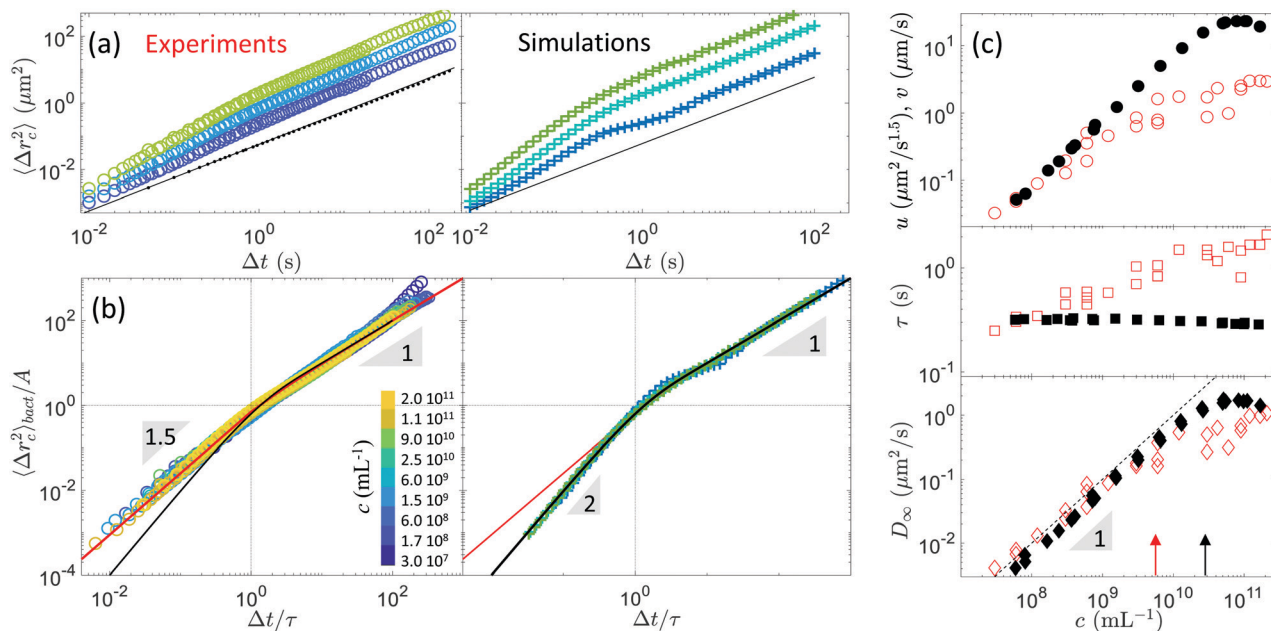
Fig. 4 Dynamics of colloids in a bath of bacteria, experiments *versus* simulation. (a) Mean square displacements of the colloids in a bath of bacteria at concentrations $c = 0.6$, 6 and 90×10^9 mL^{-1} (experiments) and $c = 0.7$, 6 and 50×10^9 mL^{-1} (simulations). For the simulations: $\ell_b = 0.5$ μm (for bacteria) and $\ell_c = 2.5$ μm (for colloids). The black line corresponds to the free diffusing colloids. (b) $\langle \Delta r_c^2 \rangle_{bact} = \langle \Delta r_c^2 \rangle - 4D_0 \Delta t$ rescaled for different concentrations of bacteria ranging from $c = 3 \times 10^7$ to 2×10^{11} mL^{-1}. The red line is an empirical fit with $\langle \Delta r_c^2 \rangle_{bact} = u \Delta t^{1.5}/(1 + \Delta t/\tau)^{0.5}$ with $D_\infty = u\tau^{0.5}/4$ and $A = u\tau^{1.5}$. The black line is the fit proposed by Wu *et al.*:[6] $\langle \Delta r_c^2 \rangle_{bact} = 4D_\infty \Delta t(1 - e^{-\Delta t/\tau})$ with $v = 4D_\infty/\tau$ and $A = 4D_\infty$. The color codes for increasing bacteria concentration c from blue to yellow. (c) Scaling of the fit parameters u, v, τ and D_∞ as a function of c: red (experiments) and black (simulations). Arrows indicate the concentration c^* that sets the upper limit of the linear regime for D_∞. The MSD simulation parameters are in agreement with the single collision simulations: $\gamma_c = k_B T/D_0(\ell_c = 2.5 \text{ μm}) = 2.75 \times 10^7$ Ns m^{-1}, $\gamma_b = 1.7 \times 10^{-7}$ Ns m^{-1}, $\varepsilon = 0.41 k_B T$ and $\Gamma = 3.35$ s^{-1}.

the effect of the bacteria, we henceforth subtract the thermal contribution to the MSD and plot $\langle \Delta r_c^2 \rangle_{bact} = \langle \Delta r_c^2 \rangle - 4D_0 \Delta t$. Remarkably, a rescaling of the displacements by a constant $A(c)$ and lag time by a time scale $\tau(c)$ collapses all curves on a single master curve, in Fig. 4(b). This master curve distinguishes two distinct asymptotic dynamics and can be empirically fitted by the function $\langle \Delta r_c^2 \rangle_{bact} = u \Delta t^{1.5}/(1 + \Delta t/\tau)^{0.5}$ with $D_\infty = u\tau^{0.5}/4$. This function interpolates between a long time diffusive dynamics where $\langle \Delta r_c^2 \rangle_{bact} = 4D_\infty \Delta t$ and a short time superdiffusive behavior where $\langle \Delta r_c^2 \rangle_{bact} = u \Delta t^{1.5}$ consistent with the early observations of Wu and Libchaber. Superdiffusion is observed over two orders of magnitude where all our experimental data collapse on the same master curve. The consistency of our short time observations dismiss the hypothesis where this regime would be a mere crossover from a ballistic to a diffusive dynamics.[6] In addition, we stress that the master curve accurately describes the transport dynamics of colloids at low bacteria concentration which further dismiss the hypothesis that the anomalous scaling law $\langle r_c^2 \rangle \sim \Delta t^{1.5}$ could be the fingerprint of collective motion.[19]

Fig. 4(c) shows the fitting parameters u, τ and D_∞ as a function of the bacteria concentration c. Those parameters increase with c. Above $c^* \sim 6 \times 10^9$ mL^{-1}, which corresponds to a bacteria volume fraction of $\sim 2\%$, u, τ and D_∞ depart from the linear regime. Only the value of D_∞ was reported in the literature and our measurements are in agreement with ref. 18 and 33. The linear evolution of D_∞ with c indicates that the diffusive process is additive: all collisions contribute independently to the dynamics.

For $c > c^*$, however, a number of bacteria collide the colloid at once, leading to a diffusive process that is no longer additive.

To gain more insight on the active transport, we simulate the dynamics of a single colloid in a bacteria bath using the model constructed in Section 3.2, and neglecting the interactions between bacteria. Noticeable similarities and differences with our experiments illustrate the nature of the origin of enhanced transport, Fig. 4(a). As in experiments, the MSD can be collapsed on a single master curve $\langle \Delta r_c^2 \rangle_{bact} = 4D_\infty \Delta t(1 - e^{-\Delta t/\tau})$,[6] Fig. 4(b). We note that the simulations and the experiments master curves are not quite identical. Both show two regimes separated by the characteristic time τ. At short time scales, the simulated MSD varies ballistically (Fig. 4(b)) corresponding to a colloid velocity v, at odds with the anomalous scaling found in the experiments. This essential difference points towards the crucial role played by the fluctuations in the bacterial dynamics on short-time superdiffusion. At long time scales, both the simulations and the experiments yield the same asymptotic behavior directly related to a diffusion process characterized by D_∞.

Given those differences and similarities between the experimental and simulated MSD, we next focus solely on D_∞. Fig. 4(c) shows the evolution of D_∞ with the bacteria concentration c. In the linear regime, experiments and simulations quantitatively agree on D_∞, indicating that the long-time enhanced diffusion is fully captured by the average scattering dynamics of the bacteria. Discrepancies appear at high concentrations. The concentration c^* where the diffusion coefficient departs from the linear regime

is much higher for simulations ($c^* \sim 2 \times 10^{10}$ mL^{-1}) and D_∞ is larger in simulations at high c. These observations indicate that the bacteria–bacteria interactions absent in the simulations are chiefly responsible for the change of regime of the effective diffusivity above c^* observed in our experiments.

4.2 Probability density function of the displacements

To further elucidate the anomalous dynamics of the colloids, we analyse the probability density function (PDF) of the colloid displacements. More quantitatively, we compute the angular average of the self part of the Van Hove function $\bar{H} = \text{PDF}_{|\Delta r_c|}/(2\pi r)$ at different lag times Δt (Fig. 5), see Section 6 for a detailed definition. $\bar{H}$ features a Gaussian center and exponential tails, which are more prominent at short times for all concentrations. At short times and low concentrations, collisions are rare events, and the Gaussian center can be unambiguously attributed to thermal noise; indeed its standard deviation σ is given by $\sigma^2 \simeq 4D_0\Delta t$ (Fig. 5(b)). At long times, many collisions have occurred and the entire distribution becomes Gaussian as a consequence of the central limit theorem; the width of the distribution is $\sigma^2 \simeq 4D_\infty\Delta t$ (Fig. 10).
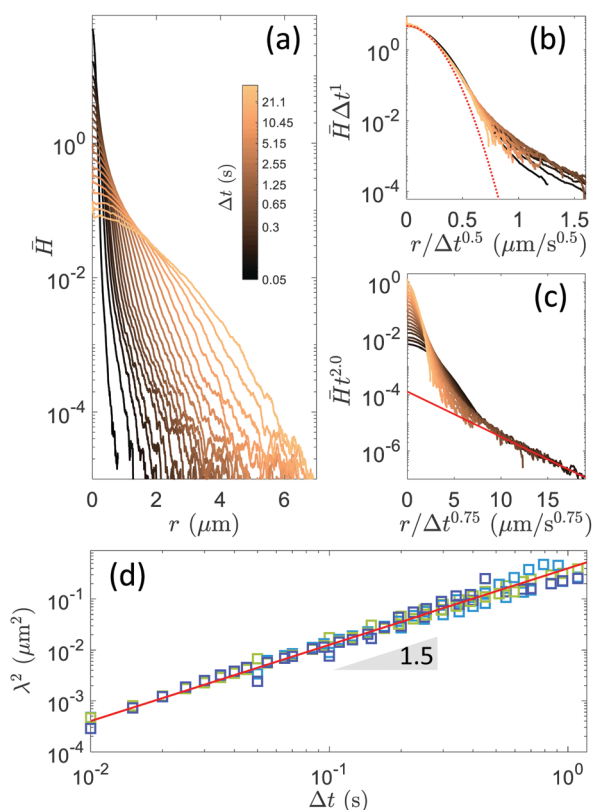

Fig. 5 Scaling of the probability distribution function of a colloid in a bath of bacteria at concentration $c = 1.2 \times 10^8$ mL^{-1}. (a) Angular average of the self part of the Van Hove function $\bar{H} = \text{PDF}_{|\Delta r_c|}/(2\pi r)$ at different lag times Δt. (b) $\bar{H}$ where r is rescaled by $\Delta t^{0.5}$. The red line corresponds to $\bar{H}$ for colloid free diffusion ($c = 0$). (c) $\bar{H}$ where r is rescaled by $\Delta t^{0.75}$. The red line is an exponential fit. (d) Square of the exponential characteristic length λ as a function of the time increment Δt for 3 concentrations of bacteria $c = 0.6$, 6 and 90×10^9 mL^{-1}. The red line is a power law of exponent 1.5.

The exponential tails are characterized by their characteristic length λ. For all concentration, at short times this length scales as $\lambda^2 \sim \Delta t^{1.5}$ (Fig. 5(c)), corresponding to the anomalous scaling of the MSD. This behavior is yet another confirmation of the existence of a genuine anomalous transport regime at short times. The numerical prefactor does not depend on the concentration (Fig. 5(d)), indicating that the exponential tails are due to the stochasticity of single-collision events, in agreement with the fact that colloids experience an average number of collisions smaller than 1 for lag times smaller than $\tau \sim 1$ s. This essential observation further demonstrates that the anomalous active transport of passive colloids dispersed in a bath of swimmers is determined by the stochastic dynamics of the swimmer-colloid interactions and therefore cannot be captured by any deterministic interaction model.

5 Concluding remarks

The pioneering discussion of active transport by Wu and Libchaber[6] led to a simple picture akin to conventional Brownian motion.[34,35] Bacteria have long been thought as playing the role of a heat bath leading to long time diffusion, and short time ballistic motion. Investigating the scattering of a single bacterium with isolated colloids, we establish that the persistence of bacteria motion does not translate in a mere ballistic displacement of the passive particles. In stark contrast, the subtle interplay between the propulsion of the swimming cell and the colloid displacement yields a genuinely anomalous and non-Gaussian dynamics. In addition, combining experiments and theory we elucidate the origin of enhanced transport showing that it chiefly relies on contact interactions and the ratio γ_c/γ_b of the drag coefficients of the colloid and the bacteria with imperceptible far-field hydrodynamic contributions of the bacteria. This last result in particular contrasts with the results of Jepson $et~al.$ which attribute enhanced diffusion to far-field advection induced by individual swimmers.[33]

The qualitative difference in the transport of colloidal bodies when activated by collisions with different swimming cells is the most prominent when comparing our experiments to that of ref. 8 and 9 where algae literally carry colloids with their swimming appendages. This diversity of microscopic interactions translates in fundamental differences in the transport statistics thereby suggesting a wealth of design strategies for cell-powered microscopic motors and heat engines.[36]

6 Methods

Microscopy

Microscopy measurements were performed with an inverted microscope (Ti-eclipse from Nikon). Images where recorded with CMOS camera (ORCA-Flash 3.0 from Hamamatsu). We use a 20$\times$ objective combined with a 1.5 magnification so that one pixel on the image represents 215 nm. We use an acquisition rate of 100 Hz. To visualize simultaneously the bacteria and the colloids, we use fluorescence and bright field. In bright field,

colloids act as a lens and focus the light in their center which enable us to track them. The light intensity of the bright field is tuned so that bacteria can also be seen simultaneously in fluorescence with gfp compatible filters.

E. coli RP437

We use a mutant *Escherichia coli* bacteria. The strain we use is *E. coli* RP437. The bacteria is modified to produce GFP (Green Fluorescent Protein) so that it is fluorescent. The bacteria is also modified to become a smooth runner, with a high persistence length, *i.e.* with a long ballistic movement and rare tumbling episodes.

E. coli preparation

E. coli are stored in a -80 °C freezer, in water (33% weight) and glycerol (66% weight). First we place a small amount of this initial mixture on an sterile agar plate (1.5%w of Aagar, 1%w of NaCl, 1%w of Tryptone, 0.5%w of Yeast Extract), with ampicillin, an antibiotic that allows us to select only our mutant. Then we put this plate in an incubator at 37 °C over the night, during which colonies originating from a single bacterium are formed. Then, an isolated colony is taken and dispersed in a liquid growth medium (1%w of NaCl, 1%w of Tryptone, 0.5%w of Yeast Extract in deionized water), in a tube permeable to oxygen, and placed in an Incu-shaker at 37 °C and 300 rpm for a night. Then, the bacteria are placed in a last growth medium (2.5 g L^{-1} of NaCl, 4 g L^{-1} of Tryptone, 4 g L^{-1} of glycerol in deionized water), and placed again in an Incu-shaker at 32 °C and 300 rpm for 4 hours. This medium, less rich in food, will force the bacteria to develop flagellas. Finally, using a syringe and a filter (Millex, MF millipore membrane 0.45 μm), we concentrate the bacteria and exchange the growth buffer with a motility buffer (67 mmol L^{-1} NaCl, 6.2 mmol L^{-1} K_2HPO_4, 3.8 mmol L^{-1} KH_2PO_4, and 0.9 mmol L^{-1} glucose).

E. coli geometrical properties

The bacteria has a radius of $\ell_b = 0.5$ μm[6] and a length of $L_b = 4.3$ μm, Fig. 6.
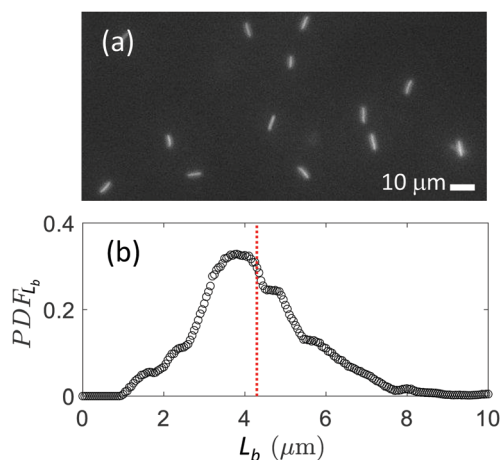

Fig. 6 Bacteria length. (a) Epifluorescence microscopy image of a dilute suspension of bacteria. (b) Probability distribution function of the bacteria length, L_b. The red line is the average bacteria length $\langle L_b \rangle = 4.3$ μm.

E. coli observation cell

Usually, the bacteria suspensions are enclosed between a glass slide and a cover slip, spaced by a paraffin film, in order to create a 100 μm gap, heated to make the cover slip adherent to the glass slide. Then, the two remaining sides of the cell are sealed using NOA61 (Norland Optical Adhesives), a liquid photopolymer that cures if exposed to ultraviolet light. This sealing is compulsory to prevent any evaporation and any parasite motion. But there is a flaw: by hermetically sealing the suspension, we prevent it from receiving oxygen from outside, and as a consequence the lifetime of the bacteria is quite short. Actually, their life expectancy depends strongly on their concentration, which directly influences the global oxygen consumption. What we find out is that for small concentration, the glass slide/cover slip device is clearly sufficient, but for higher concentration, the mean velocity of the bacteria decreases from 10 μm s^{-1} to 2 μm s^{-1} in less than five minutes, which forbids us to lead experiments with a high concentrated bacteria bath. To prevent this problem we developed an agar observation cell. Once heated in water, agar dissolves and forms, after a few minutes of cooling, a gel. As a gel, it constitutes a porous medium, and therefore lets the oxygen penetrate its structure. The porosity of the gel is related to the concentration of agar. Typically, we use a concentration of 15 g mL^{-1}. We fill a plastic Petri dish with agar dissolved in the motility buffer, and wait for the gel to solidify. Then, we extrude a cylinder of agar, and place our bacteria suspension into the well previously created. To prevent any parasite motion in the solution, we place an agar cover on the top of the well, so that the bacteria solution does not evaporate. We take care to avoid any bubble formation under the cover. The bacteria and colloid dynamics are observed using microscopy at the bottom the agar observation cell. Given that the colloids sediment to the bottom of the cell, the colloid dynamics is quasi two dimensional.

E. coli motility lifetime

To measure the motility lifetime of the bacteria dispersions we use differential dynamic microscopy (DDM). Indeed, when the concentration of bacteria is high, typically at least 10^9 mL^{-1}, it is impossible to focus on single trajectories in order to deduce bacteria velocity. Therefore, we need a technique to measure a mean velocity without having to look at individual motion. This is where the DDM comes into play.[25,26] Using DDM, we measure, as in a dynamic light scattering, the intermediate scattering function $f(q, \Delta t)$ where q is the scattering wave number and Δt is the time increment, Fig. 7a. Fitting f with the appropriate model gives access to properties of the bacteria dispersion.

The model we use is described in ref. 25, 26 and 37. It models a population of bacteria as straight swimmers with a speed distribution and isotropic directions. Each bacteria also undergoes Brownian motion. The model contains a fraction α of motile cells and $(1 - \alpha)$ of non-motile cells. The model yields the ballistic time τ_b related to the bacteria average velocity $\langle v_b \rangle$ and the diffusive time τ_d related to the brownian diffusion coefficient of the bacteria D_b, as well as the fraction of motile
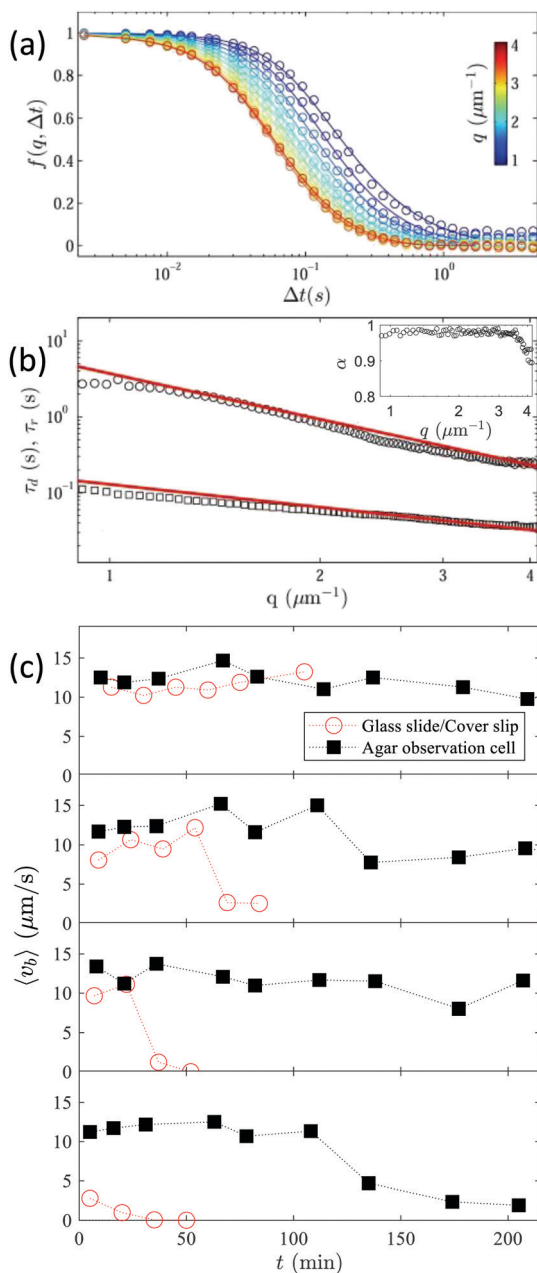
Fig. 7 DDM experiment on bacteria suspensions of concentration c. (a) Intermediate scattering function f calculated from the DDM experiment (circles) and its fit (solid line) for various scattering number q. $c = 1.8 \times 10^{10}$ mL^{-1}. (b) Characteristic diffusion time τ_d (circles) and ballistic time τ_r (square) as a function of q extracted from the fit of f in (a). $\langle v_b \rangle = 1/(q\tau_r) = 10.1$ µm s^{-1} and $D_d = 1/(q\tau_d^2) = 0.31$ µm^2 s^{-1} in agreement with.[33] Inset: motility fraction α as a function of q. On average $\alpha = 0.98$. (c) Comparison of the average velocity of bacteria measured using DDM for four different concentrations $c = 1.8, 4.5, 9$ and 18×10^{10} mL^{-1} (top to bottom) between the agar observation cell and conventional glass cell.

bacteria α, Fig. 7b. With this model, the motility of the bacteria dispersion is quantified by the two parameters $\langle v_b \rangle$ and α. The results presented in this paper are obtained with bacteria dispersions such that $\langle v_b \rangle > 10$ µm s^{-1} and $\alpha > 0.9$. Fig. 7a and b display typical DDM results obtained from such a dispersion. To measure the

motility lifetime of a bacteria dispersion we focus specifically on $\langle v_b \rangle$. Indeed, when $\langle v_b \rangle > 10$ µm s^{-1}, $\alpha > 0.85$. However, when $\langle v_b \rangle$ drops α may remain high.

Fig. 7c shows the time evolution of $\langle v_b \rangle$ for the glass observation cell and the agar observation cell. If there is a drop in the velocity, it means that bacteria have less energy to move and start to become non-motile. As a consequence, we can compare the effectiveness of the two setups by comparing both the mean velocity as a function of time. At low concentrations both observation cells are equivalent, and we do not face any motility problems. Nevertheless, as we increase the concentration, we see the limitations of the hermetic glass slide/cover slip cell. In less than 30 minutes for a concentration of 15×10^9 bacteria per mL, the velocity drops to almost zero, and for the higher concentrations, the sealing of the cell with the NOA61 takes too much time to make the observation of the bacteria possible before they start becoming unmotile. On the contrary, the agar cell increases substantially the bacteria motility lifetime, and allows us to study concentrated bacteria suspensions in a stationary regime over a period of 1 h for all concentrations tested in this article.

E. coli concentration

The bacteria concentration is determined using the optical absorbance OA$_{600}$ at 600 nm measured with an UV-visible spectrometer (ocean optics, USB4000) where $c = 1.2 \times 10^9$ OA$_{600}$.[22] OA = $\log_{10}(I_0/I)$ where I_0 is the solvent transmitted intensity and I is the bacteria dispersion transmitted intensity. Bacteria are known to have higher density near walls. To measure the bacteria concentration profile along the z – direction in the agar observation cell, we use a confocal spinning disk microscope, that allows us to visualize a z – plan of the well with a vertical focal depth of 8 µm, z – step of 2.5 µm at 0.1 Hz. In Fig. 8, we use a bacteria suspension at a very low concentration, so that we are able to count individual bacteria at different heights. At the same time, we calculate the mean intensity of these very same images. As expected, we find that the fluorescent intensity is directly proportional to the number of bacteria. First of all, the profile is very similar to
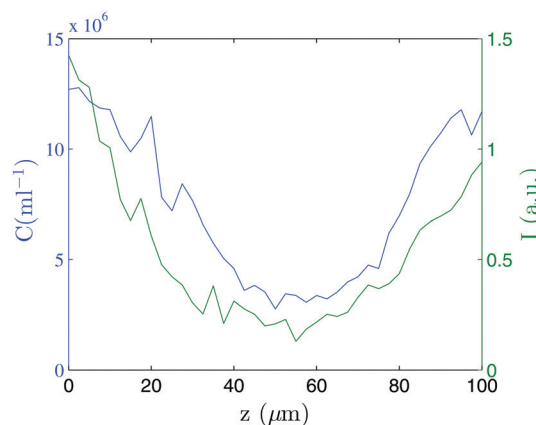

Fig. 8 Bacteria concentration profile along the z – axis. Profile of bacteria concentration in the agar observation cell along a vertical axis (z – axis), measured by counting the bacteria (blue), and averaging the bacteria fluorescence intensity I (green) in the same experiment.

what we can find in literature, in ref. 27 for example. We find again that bacteria are attracted to surfaces. As a consequence, we can see that the concentration near a surface is far higher than the mean concentration that we measure thanks to optical absorption. In all our experiments, we need to correct the concentration we measure by optical density by an adjustment factor to take into account this spatial inhomogeneity. As the colloids we use diffuse at the bottom surface of the agar observation cell, we measure the concentration c of the bacteria in this region of interest. Experimentally, we find that the bacteria concentration is 5 times higher at the bottom of the observation cell than the average concentration measured with optical density. As a consequence, since we realize all our experiments near the surface of the agar device, we will multiply all the concentration we measure by 5.

E. coli velocity

Single bacteria dynamics is obtained by tracking individual bacteria and identify their center of mass $r_b(x_b, y_b)$ and their orientation defined by the angle θ_b between the long axis of the bacteria and the x – axis of the laboratory. We then compute $|\Delta r_b| = |r_b(t + \Delta t) - r_b(t)|$ the norm of the displacement increment of the bacteria position as a function of the time t and the time increment Δt. Fig. 9 shows the distribution function of the norm of the position increment $|\Delta r_b|$ scaled as a function of $|v_b|$. Measurements are averaged over 200 bacteria. For $\Delta t > 0.2$ s, all curves collapse on a master curve centered on a Gaussian of average value $\langle v_b \rangle =15$ µm s^{-1} with a standard deviation of 4 µm s^{-1}. This behavior is obtained on the entire range of concentrations tested in the paper. For high concentrations only a few percent of the bacteria were fluorescently labeled to allow tracking.

Colloids distribution function

Since our problem is isotropic, the probability density function of the displacements should be of the form $H(x, y) = \bar{H}\left(\sqrt{x^2 + y^2}\right)$.
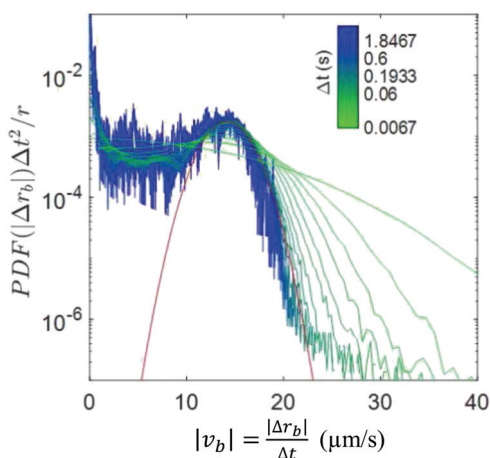
Fig. 9 Bacteria velocity. Velocity distribution function as a function of v_b. Color codes for time. The red line is a Gaussian distribution centered on $\langle v_b \rangle = 15$ µm s^{-1}. The standard deviation is 4 µm s^{-1}.
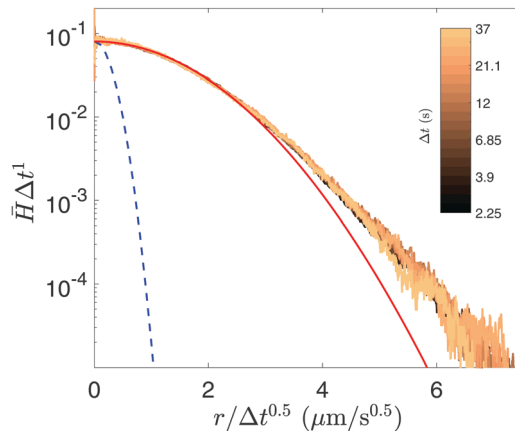
Fig. 10 Scaling of $\bar{H}$ of the colloids as a function of $r/\Delta t^{0.5}$ for $\Delta t > \tau$ in a bath of bacteria at $c = 90 \times 10^9$ mL^{-1}. Dash blue line: free diffusion of the colloids ($c = 0$). Red line: best Gaussian fit for $r/\Delta t^{0.5} < 2$ µm s$^{-0.5}$.

$\bar{H}(r)$ is the angular average of the two-dimensional PDF $H(x,y)$; it is related to the PDF of the norm of the displacement $g(r)$, by $\bar{H}(r) = g(r)/(2\pi r)$. Usually, the marginal distributions $\int H(x, y)dy$ or $\int H(x, y)dx$ are plotted. If $H(x,y)$ is Gaussian, the marginal distributions are also Gaussian; however, if $H(x,y)$ is not Gaussian, the marginal distributions do not represent the radial dependence of $H(x,y)$ in a straightforward way. For this reason, we choose here to work with $\bar{H}(r)$ (Fig. 10).

Conflicts of interest

There are no conflicts to declare.

Acknowledgements

Notes and references

1 A. Sokolov, M. M. Apodaca, B. A. Grzybowski and I. S. Aranson, *Proc. Natl. Acad. Sci. U. S. A.*, 2010, **107**, 969–974.
2 R. Di Leonardo, L. Angelani, D. Dell'Arciprete, G. Ruocco, V. Iebba, S. Schippa, M. Conte, F. Mecarini, F. De Angelis and E. Di Fabrizio, *Proc. Natl. Acad. Sci. U. S. A.*, 2010, **107**, 9541–9545.
3 C. Maggi, J. Simmchen, F. Saglimbeni, J. Katuri, M. Dipalo, F. De Angelis, S. Sanchez and R. Di Leonardo, *Small*, 2016, **12**, 446–451.
4 A. Aubret, M. Youssef, S. Sacanna and J. Palacci, *Nat. Phys.*, 2018, **14**, 1114.
5 S. Ramananarivo, E. Ducrot and J. Palacci, *Nat. Commun.*, 2019, **10**, 1–8.
6 X.-L. Wu and A. Libchaber, *Phys. Rev. Lett.*, 2000, **84**, 3017.

7 C. Bechinger, R. Di Leonardo, H. Löwen, C. Reichhardt, G. Volpe and G. Volpe, *Rev. Mod. Phys.*, 2016, **88**, 045006.

8 K. C. Leptos, J. S. Guasto, J. P. Gollub, A. I. Pesci and R. E. Goldstein, *Phys. Rev. Lett.*, 2009, **103**, 198103.

9 R. Jeanneret, D. O. Pushkin, V. Kantsler and M. Polin, *Nat. Commun.*, 2016, **7**, 12518.

10 L. Ortlieb, S. Rafaï, P. Peyla, C. Wagner and T. John, *Phys. Rev. Lett.*, 2019, **122**, 148101.

11 A. J. Mathijssen, R. Jeanneret and M. Polin, *Phys. Rev. Fluids*, 2018, **3**, 033103.

12 C. Valeriani, M. Li, J. Novosel, J. Arlt and D. Marenduzzo, *Soft Matter*, 2011, **7**, 5228–5238.

13 D. O. Pushkin and J. M. Yeomans, *J. Stat. Mech.: Theory Exp.*, 2014, **2014**, P04030.

14 J.-L. Thiffeault, *Phys. Rev. E: Stat., Nonlinear, Soft Matter Phys.*, 2015, **92**, 023023.

15 A. Morozov and D. Marenduzzo, *Soft Matter*, 2014, **10**, 2748–2758.

16 E. W. Burkholder and J. F. Brady, *Phys. Rev. E*, 2017, **95**, 052605.

17 L. F. Cugliandolo, G. Gonnella and A. Suma, *Phys. Rev. E*, 2015, **91**, 062124.

18 D. O. Pushkin and J. M. Yeomans, *Phys. Rev. Lett.*, 2013, **111**, 188101.

19 G. Grégoire, H. Chaté and Y. Tu, *Phys. Rev. E*, 2001, **64**, 011902.

20 G. Miño, T. E. Mallouk, T. Darnige, M. Hoyos, J. Dauchet, J. Dunstan, R. Soto, Y. Wang, A. Rousselet and E. Clement, *Phys. Rev. Lett.*, 2011, **106**, 048102.

21 A. E. Patteson, A. Gopinath, P. K. Purohit and P. E. Arratia, *Soft Matter*, 2016, **12**, 2365–2372.

22 J. Schwarz-Linek, J. Arlt, A. Jepson, A. Dawson, T. Vissers, D. Miroli, T. Pilizota, V. A. Martinez and W. C. Poon, *Colloids Surf., B*, 2016, **137**, 2–16.

23 J. C. Crocker and D. G. Grier, *J. Colloid Interface Sci.*, 1996, **179**, 298–310.

24 R. Cerbino and V. Trappe, *Phys. Rev. Lett.*, 2008, **100**, 188102.

25 D. Germain, M. Leocmach and T. Gibaud, *Am. J. Phys.*, 2016, **84**, 202–210.

26 V. A. Martinez, R. Besseling, O. A. Croze, J. Tailleur, M. Reufer, J. Schwarz-Linek, L. G. Wilson, M. A. Bees and W. C. Poon, *Biophys. J.*, 2012, **103**, 1637–1647.

27 A. P. Berke, L. Turner, H. C. Berg and E. Lauga, *Phys. Rev. Lett.*, 2008, **101**, 038102.

28 D. Takagi, J. Palacci, A. B. Braunschweig, M. J. Shelley and J. Zhang, *Soft Matter*, 2014, **10**, 1784–1789.

29 S. E. Spagnolie, G. R. Moreno-Flores, D. Bartolo and E. Lauga, *Soft Matter*, 2015, **11**, 3396–3411.

30 O. Sipos, K. Nagy, R. Di Leonardo and P. Galajda, *Phys. Rev. Lett.*, 2015, **114**, 258104.

31 H. Shum and J. M. Yeomans, *Phys. Rev. Fluids*, 2017, **2**, 113101.

32 S. Chattopadhyay, R. Moldovan, C. Yeung and X. Wu, *Proc. Natl. Acad. Sci. U. S. A.*, 2006, **103**, 13712–13717.

33 A. Jepson, V. A. Martinez, J. Schwarz-Linek, A. Morozov and W. C. Poon, *Phys. Rev. E: Stat., Nonlinear, Soft Matter Phys.*, 2013, **88**, 041002.

34 R. Huang, I. Chavez, K. M. Taute, B. Lukić, S. Jeney, M. G. Raizen and E.-L. Florin, *Nat. Phys.*, 2011, **7**, 576–580.

35 A. P. Hammond and E. I. Corwin, *Phys. Rev. E*, 2017, **96**, 042606.

36 S. Krishnamurthy, S. Ghosh, D. Chatterji, R. Ganapathy and A. K. Sood, *Nat. Phys.*, 2016, **12**, 1134–1138.

37 G. Stock and T. Jenkins, *Biophys. J.*, 1978, **22**, 79–96.